https://doi.org/10.3311/PPci.46484
Creative Commons Attribution

Periodica Polytechnica Civil Engineering

Surrogate Model for Rubber Spring and Damping Elements Based on High-fidelity Simulations of Cyclically Loaded Vulcanizates

Robert Eberlein[1*], Thomas Mayer[1], Sven Düzel[1], Paolo Capozzi[1], Claus Wrana[2]

[1] ZHAW Institute of Mechanical Systems, Technikumstr. 9. CH-8401 Winterthur, Switzerland
[2] Compounds AG, Barzloostr. 1, CH-8330 Pfäffikon, Switzerland
[*] Corresponding author, e-mail: robert.eberlein@zhaw.ch

Received: 18 September 2026, Accepted: 25 October 2026, Published online: 02 November 2026

Abstract

This paper presents a surrogate modeling approach for predicting the cyclic stiffness characteristics of rubber spring and damping elements (RSDE) used in vibration isolation systems. The methodology is based on high-fidelity finite element (FE) simulations that incorporate geometry-dependent assembly effects and advanced material modeling of filled vulcanizates subjected to cyclic loading. The constitutive framework combines the Modified Extended Tube Model (METM) with Advanced Mullins Damage Modeling (AMDM), providing a physically motivated description of hyperelasticity, stress softening, and steady-state hysteretic behavior. The resulting three-dimensional FE implementation was realized as an Abaqus user material subroutine and validated against experimental measurements of commercial RSDE. Simulated torque-angle characteristics showed excellent agreement with experiments, with peak torque deviations below ±3%.

To enable rapid engineering predictions, a parameterized FE model covering representative RSDE geometries was used to generate a design-of-experiments dataset. The simulated loading characteristics were condensed into three physically interpretable parameters describing cyclic stiffness behavior and subsequently approximated using multi-linear response surface regression models. The surrogate model links six geometric design variables to the non-linear torque-angle response, achieving high predictive accuracy with adjusted coefficients of determination R^2_{adj} up to 0.977. Analysis of the regression model reveals the influence of rubber cord dimensions and profile geometry on stiffness evolution under torsional loading. Comparison with independent test cases demonstrates that the surrogate model reliably reproduces FE predictions within the considered design space. The proposed surrogate model enables real-time estimation of geometry- and material-dependent cyclic stiffness characteristics, supporting efficient design and optimization of customized RSDE applications without testing.

Keywords

vulcanizates/rubber compounds, cyclic loading/dynamic behavior, high-fidelity simulation, surrogate model

1 Introduction

Rubber spring and damping elements (RSDE) are frequently applied in various industrial applications for the support and damping of vibrating and motion systems such as vibrating conveyor or sieving systems, motor mounts or crushers for e.g. the mining, agricultural, or food and beverage sectors as well as in robotics for high-impact shock absorption and energy storage in dynamic legged locomotion [1, 2, 3]. They consist of an inner and outer square steel profile which are linked by compressed rubber cords, see Fig. 1. RSDE feature a dominant torsional Degree of Freedom (DoF) and are often interconnected in a pantograph-structure, forming a rubber spring and damping system (RSDS) providing a redominantly vertical DoF, see Fig. 1.

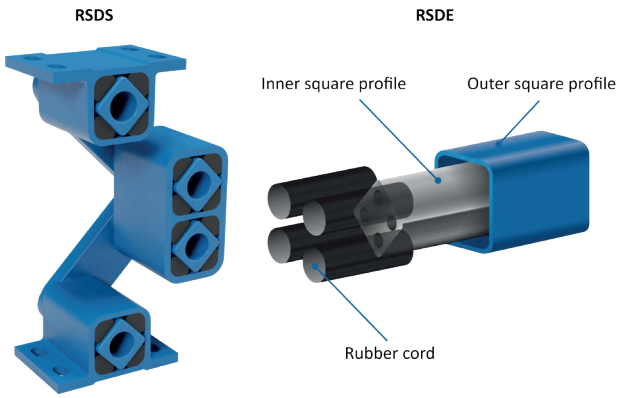


Fig. 1 ROSTA rubber spring and damping system (RSDS) consisting of basic rubber spring and damping elements (RSDE)

Cite this article as: Eberlein R., Mayer, T., Düzel, S., Capozzi, P., Wrana, C. " Surrogate Model for Rubber Spring and Damping Elements Based on High-fidelity Simulations of Cyclically Loaded Vulcanizates", Periodica Polytechnica Civil Engineering, 2026. https://doi.org/10.3311/PPci.46484

For the design, analysis, and optimization of vibrating systems detailed knowledge of hysteretic behavior as well as the underlying cyclic stiffness and damping properties of the RSDE is essential for the prediction of the loading characteristics of the parent RSDS. While experimental determination is time consuming and expensive, analytical approaches fall short due to the physical complexity. Unlike conventional metallic springs or hydraulic dampers, the non-linear nature of the mechanical loading response of elastomers does not allow for an analytical estimation of the mechanical characteristics of RSDE. In addition to a strong dependency of the mechanical performance of RSDE on the mixture of the elastomeric compound, the geometrical design of the RSDE plays a crucial, yet complex role. These challenges in analytically handling the complex mechanical behavior of RSDE currently limit the development of optimized, customer-specific solutions.

A digital model [4] of a pre-screening system employing RSDS was developed recently, describing its screening efficiency for different operation conditions [1]. Further improvement of the model performance was stated to require detailed knowledge of the non-linear cyclic stiffness and damping properties of the RSDS employed within the pre-screening system. As these are constructed from several RSDE, the loading characteristics of RSDS can be derived from the RSDE properties together with non-linear analytical equations of motion. This has been attempted by [5] using limited catalogue data of the manufacturer ROSTA AG. Similarly, RSDS properties at the operation point were directly predicted by [6] using linearized analytical equations of motion. Generalizability of these models is limited using catalogue data without experimental calibration or validation. In addition, linearization of the equations of motions must be repeated at each working point, separately. Furthermore, improved accuracy can only be achieved through consideration of the non-linear RSDS properties, limiting the applicability of this approach. A mere loading direction dependent non-linearity does, however, not cover the complexity of the elastomeric compound. In [7] a more reliable non-linear modelling approach is presented, using the MathWorks Simulink simulation framework to build a non-linear spring and damping model of the RSDE as rotational joint. The calibration of experimental data provided by the manufacturer ROSTA AG highlights the advantages of a non-linear approach and shows the difficulty to incorporate effects like material softening under cyclic loading. Still, the model presented does not account for the geometry of the RSDE. Eventually, Finite Element (FE) based modelling offers a suitable numerical approach to analyze the cyclic stiffness and damping properties of RSDE without producing prototypes and performing experimental tests [8, 9]. Reliable FE model predictions require detailed analysis of the material behavior of vulcanizates and the consideration of the assembly process defining internal stress states of the rubber cords to reproduce the experimentally observed behavior. Stress states thereby depend on the dimensions of the rubber cord itself as well as the adjacent inner and outer square profiles [10].

While there is a clear need for the respective industries to predict, analyze, and optimize the mechanical response of RSDE and RSDS, the use of high-fidelity FE simulations is limited by their computational costs as well as the required expert knowledge. For the appropriate design of vibrating systems using RSDS, a computationally efficient and readily accessible tool is needed that allows to reliably predict key mechanical parameters such as RSDE stiffness and damping properties. In similar contexts, surrogate models have been employed to replace computationally expensive high-fidelity FE simulations allowing fast predictions of expected mechanical responses for varying geometries. For instance, advanced statistical modeling and machine learning techniques such as Kriging have been used to predict entire load-displacement curves of carbon fiber reinforced polymer/aluminum alloy multi-riveted-bonded joints with varying geometries [11]. Similarly, a Neural Network has been employed by [12] to predict the non-linear mechanical response of lattice structures with varying strut diameters under large displacements. In both cases, computationally expensive high-fidelity FE simulations were replaced by fast running but rather complex statistical models at high levels of the coefficient of determination larger than 0.93. Simpler statistical models such as multiple linear regression models [13, 14] have further been applied to characterize the effect of uncertainties in the elastic modulus on the mechanical response of a truss structure using a modified response surface method [15].

This paper presents a surrogate modelling approach for the non-linear mechanical response of RSDE to torsional loading based on simple multiple linear regression. The surrogate model is trained on data from high-fidelity FE simulations that account for the mixture-specific steady-state hyperelastic behavior of vulcanizates after multiple loading cycles under varying RSDE geometries. In addition, a parametric model is adopted to represent the non-linear mechanical response. The surrogate model thereby

consists of three separate multiple linear regression models that predict the free parameters of the mechanical response characteristic as a function of geometrical input variables. This allows the use of a simple regression-based surrogate rather than more complex machine learning models.

The approach combines advanced FE-based simulation models for a torsional RSDE with a novel material modelling approach [16, 17, 18] linking the physical properties of the rubber compound to material parameters, enabling mixture-dependent non-linear material response under cyclic loading conditions, validated by experimental tests. The surrogate model provides realistic geometry and material dependent predictions of the cyclic stiffness properties of RSDE. This enables engineers to access mechanical characteristics of optimized and/or customized RSDE and RSDS in real time without the need for expensive prototype testing.

2 Approach

2.1 Constitutive model and FE implementation

The constitutive model and finite element (FE) implementation are built upon two closely related material modelling concepts: (1) the Modified Extended Tube Model (METM) as a physically motivated constitutive model for filled vulcanized elastomers, establishing a direct relationship between compound composition, filler content, molecular network structure, and mechanical behavior [16]; (2) through Advanced Mullins Damage Modeling (AMDM), providing a theory and parameter identification procedure for the description of stress softening and hysteresis after multiple loading cycles [17]. The present work integrates both concepts into a fully three-dimensional finite element framework suitable for industrial applications and high-fidelity simulations.

A central motivation of the constitutive concept is the limitation of conventional hyperelastic material models used in elastomer engineering. Although phenomenological strain-energy functions can often reproduce measured stress–strain curves, they usually lack a direct connection to the underlying material formulation. As a result, FE simulations may predict component behavior, but they provide only limited guidance for the design and optimization of rubber compounds themselves. In contrast, the METM developed by [16] is physically motivated, separates the contributions of the chemical crosslinked network as well as the entanglement network and introduces a reinforcement function for accurately describing filler content such as carbon black, thereby enabling a more meaningful interpretation of material parameters. The subsequent extension through AMDM [17] additionally allows the description of cyclic softening and steady-state material behavior after repeated loading.

The FE implementation [18] is formulated within the framework of non-linear continuum mechanics under isothermal conditions. The governing equations consist of the balance of linear momentum, kinematic relations, boundary conditions, and METM as well as AMDM based constitutive equations. Since large deformations occur in elastomeric components, analytical solutions are generally not available. Therefore, the weak form of equilibrium is derived using the Principle of Virtual Displacements and solved numerically by non-linear finite elements. The resulting non-linear system is linearized through a consistent Newton–Raphson procedure, requiring not only stresses but also the corresponding material tangent tensors for quadratic convergence.

For numerical implementation, the originally incompressible METM and AMDM formulations are extended by introducing a volumetric energy contribution dependent on the Jacobian of the material deformation gradient. This modification ensures mathematical soundness and permits the application of three-dimensional continuum elements. The second Piola–Kirchhoff stress tensor is derived directly from the strain-energy function, and the corresponding fourth-order material tensor is obtained through second derivatives of the energy potential (strain-energy function). Spectral decomposition techniques are employed to express stresses and tangent moduli in principal directions, facilitating robust numerical implementation within the FE environment.

A major advancement of the constitutive model and FE implementation is the incorporation of the relaxation-based stress approach proposed by [17]. Experimental observations demonstrate that elastomers subjected to repeated cyclic loading approach an equilibrium (steady-state) stress–strain response that differs significantly from the virgin material behavior. To capture this phenomenon, a relaxation function is introduced that scales the original strain-energy density and stress response. The relaxed METM formulation requires the derivation of modified stress expressions and consistent tangent operators. Volume-preserving deformation measures are introduced, and relaxed stresses are decomposed into contributions from the chemical network, molecular entanglements, and volumetric deformation. Corresponding expressions for the tangent stiffness matrix are derived analytically to

ensure numerical stability and convergence in non-linear FE simulations. These derivations form the foundation of the Abaqus user material implementation presented in [18].

The second key component is AMDM. Traditional Mullins damage models, such as the widely used pseudo-elastic formulation of [19], assume that all damage is generated during the first loading cycle and that subsequent cycles follow a fixed damaged response. According to AMDM, this assumption does not adequately represent experimentally observed behavior, especially after multiple cyclic deformations. AMDM addresses this limitation by introducing two distinct damage functions. One function describes the increasing branch of a loading cycle, while a second function governs the decreasing branch. This distinction allows the model to reproduce the different damage evolution mechanisms associated with loading and unloading. The damage functions depend on the relaxed strain-energy density and its curvature, enabling the model to represent progressive stress softening and hysteresis over multiple deformation cycles. The resulting formulation provides a significantly improved description of the equilibrium behavior observed experimentally in filled elastomers.

In summary, the physically motivated METM and AMDM material modelling concepts extend both into a comprehensive three-dimensional FE framework. The complete FE implementation was realized as a user material subroutine (UMAT) in Abaqus Standard [18]. Because solid elastomers exhibit quasi-incompressible behavior, the Abaqus Hybrid Formulation was employed together with hybrid solid elements. Numerical studies involving RSDE demonstrated that the model accurately predicts load–deformation curves, including the influence of stress relaxation and cyclic damage. The simulations reproduced experimentally, observed torque-angle relationships within manufacturing tolerances and showed robust convergence behavior. Unlike conventional phenomenological approaches, the material modelling concepts establish a direct link between elastomer compound formulation and component performance, thereby enabling predictive high-fidelity FE simulations.

2.2 High-fidelity RSDE simulation model

RSDS are composed of various interconnected RSDE, see Fig. 1. Thus, the mechanical characteristics of the RSDS are essentially determined by the characteristics of the building-block RSDE which is the focus of the advanced parametrized high-fidelity FE model.

The predominating load case consists of a torsional loading of the inner square profile of the RSDE up to a rotational angle of ±30°. To achieve good agreement between measured and simulated torsional loading – rotation angle characteristics, it is decisive to accurately model the assembly of the rubber cords into the RSDE determining their internal stress state in the unloaded 0° condition which determines the torsional stiffness characteristic. Likewise, appropriate material states must be prescribed during assembly and subsequent torsional loading to +30° and unloading to 0° as well as reverse loading to -30° and unloading to 0° according to Table 1. Thereby, three different states need to be considered: 1) relaxed, 2) damaged / loading, and 3) damaged / unloading. The different simulation steps are summarized in Fig. 2.

In a first step (1. Pressing), the four rubber cords are pressed between inner and outer square profiles. To achieve a stable, converging simulation, an interference fit is applied to the rubber cord surface shifting the surface nodes towards the target inner and outer contact surfaces along the normal direction. Thereby, a two-fold symmetry condition is imposed as kinematic boundary condition to the rubber cord. Emulating the effect of a lubricant typically applied during real assembly, this process is further assumed to be frictionless. In the following step (2. Stretching), an axial displacement S_{GK} is applied to the front and back side of the rubber cord to realize an effective assembled length with the associated degree of compression. Therefore, both symmetry and frictionless contact are assumed. A relaxed material state is defined for the first two assembly steps.

Table 1 Material states and friction coefficients prescribed for different simulation steps

Step	Torsion Angle [deg]	Material State [-]	Friction Coefficient [-]
Pressing	0°	Relaxed	0
Stretching	0°	Relaxed	0
Model Change	0°	Relaxed	0.5
Pre-Damage	±30°	Relaxed	0.5
Torsion Up	0° to +30°	Damaged / Loading	0.5
Torsion Unload	+30° to 0°	Damaged / Unloading	0.5
Torsion Down	0° to -30°	Damaged / Loading	0.5
Torsion Unload	-30° to 0°	Damaged / Unloading	0.5

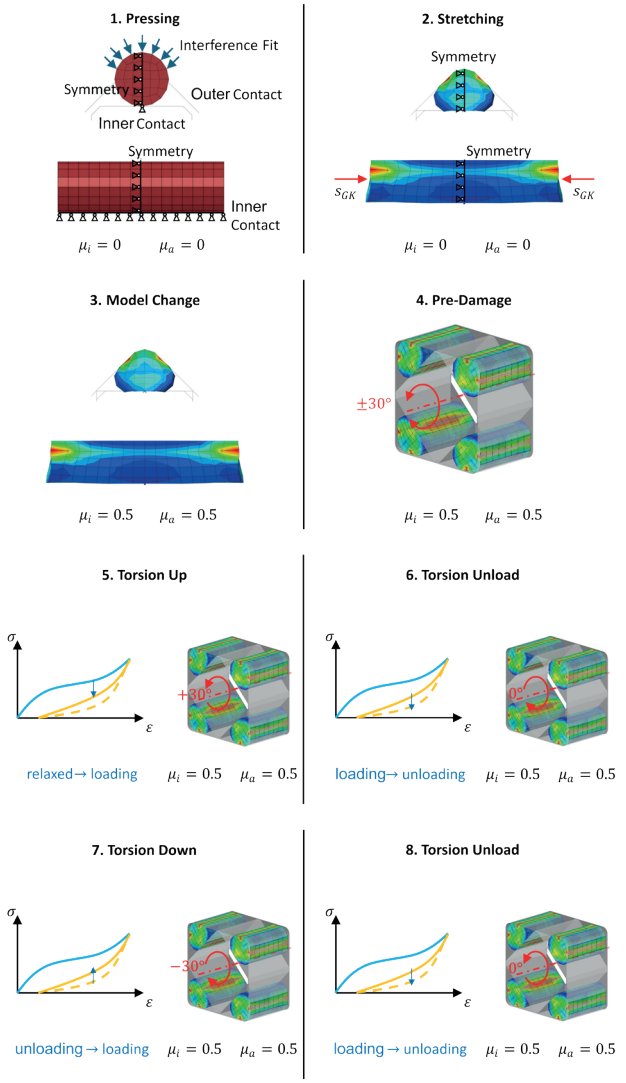


Fig. 2 Loading steps for torsional load-case for high-fidelity RSDE simulation

In step 3, a model change is applied setting the friction coefficients at the inner and outer contact surfaces (μ_i and μ_a, respectively) to 0.5, while releasing the symmetry condition as the position of the rubber cords is well defined by the established contact. In the following step 4, the limiting damage state is determined from the strain states obtained during the maximum angular deflection of ±30° [17]. This yields the information required to obtain the local as-damaged material state for loading and unloading conditions needed to realistically model the steady-state mechanical behavior of the RSDE for cyclic torsional loading with ±30°. Thereby, the material states during an increase of the rotational angle in either direction is a damaged/loading, while any reduction of the rotation angle towards zero is a damaged/unloading material condition.

As described above, the 3D simulation model is set up in the commercial FE software Abaqus by Dassault Systemes using a user-material subroutine (UMAT). Inner and outer square profiles were assumed to be analytical rigid surfaces with infinite length. The boundary conditions are applied via a reference point tied to the respective rigid bodies. The four rubber cords were discretized with fully integrated linear C3D8H HEX elements with hybrid formulation supporting quasi-incompressible material behavior of the rubber cords by avoiding volumetric locking.

To investigate and efficiently simulate the loading response characteristics (torque vs. rotation angle) for varying geometries, the model was fully parameterized according to Fig. 3. The outer and inner square profiles are defined based on three parameters, i.e. width of inner profile B_{IT}, width of outer profile B_{AT}, and the corner radius of outer profile R_{AT}. The rubber cords were further fully defined by another three parameters, i.e. the diameter of the rubber cords D_{GK} as well as the as-cut length L^S_{GK} and the effective assembled length L^e_{GK}. For this study, the material was fixed for one specific compound, i.e. Rubmix 10M by ROSTA AG.

2.3 Surrogate model

The goal of the developed surrogate model is to provide reliable information on representative cyclic stiffness properties of RSDE for varying geometries without the need of time-consuming simulations. For this purpose, an extensive dataset with loading response characteristics (torque vs. rotation angle) for varying RSDE geometries was created using the high-fidelity FE based simulation presented earlier. Following a Central Composite Face-Centered design of experiment (DoE) [20], a total of 45 different configurations for training and 8 for testing were generated and used to establish a multi-linear regression model.

Variation ranges of geometrical parameters were defined as representative of the ROSTA DR40 to DR60 RSDE family while geometrical feasibility limits were accounted for. Due to geometrically induced limitations, the feasibility

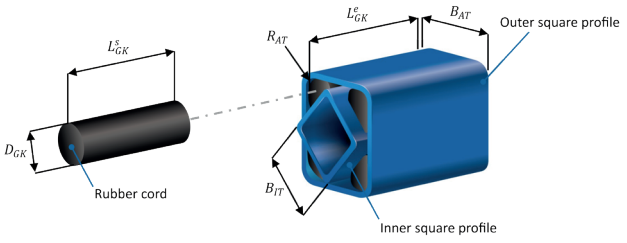


Fig. 3 Geometrical parametrization of RSDE model

Table 2 Approximate limiting minimum and maximum values [mm] for geometrical parameters in DoE

B_{IT}	B_{AT}	R_{AT}	D_{GK}	L^S_{GK}	L^e_{GK}
40	54	5.5	18	25	34
60	90	25.0	41	270	300

limits vary strongly with B_{IT}. Each geometrical parameter was varied on three levels within their respective feasibility limits. Test cases were chosen only inside the parameter regimes covered by the training data, thus checking the interpolation performance of the final model. Due to confidentiality, only the limiting maximum and minimum values independent of B_{IT} are given in Table 2. Simulations were stable for cases where the volume ratio of rubber cord to geometrically available volume between inner and outer profile, i.e. a measure of the degree of compression, was between 0.75 to 0.90.

After the simulation of the various RSDE geometry variants, the loading response characteristics for a rotational angle of up to ±30° was extracted. To simplify the complexity of the dataset, an average torque vs. rotation curve was determined from the absolute values of the loading and unloading characteristics, generating a point-symmetric curve for positive and negative rotation angles, see Fig. 4. Subsequently, the slope of the torque vs. rotation curve was calculated and fitted with the following erf-approach:

$$\frac{dM_t}{d\alpha} = a + 0.5 \cdot d \cdot \left(1 + \mathrm{erf}\left(\frac{\sqrt{\pi}}{2 \cdot b} \cdot (\alpha - c)\right)\right) \tag{1}$$

The averaged torque M_t vs. rotation angle α curve is recovered by integrating Eq. (1) using the fitted model parameters a, b, c, and d. The advantage of this approach lies in the interpretability of the parameters as outlined in Fig. 5.

- a averaged slope / stiffness at $\alpha \to -\infty$, at $\alpha = 0°$ the slope is roughly 1.1α
- b measure of the curvature and thereby the sharpness of the transition from slopes a to d
- c angle at maximum curvature, kept constant at $c = 30°$
- d averaged slope / stiffness at $\alpha \to +\infty$, at $|\alpha| = 30°$ the slope is $a + \frac{d}{2}$

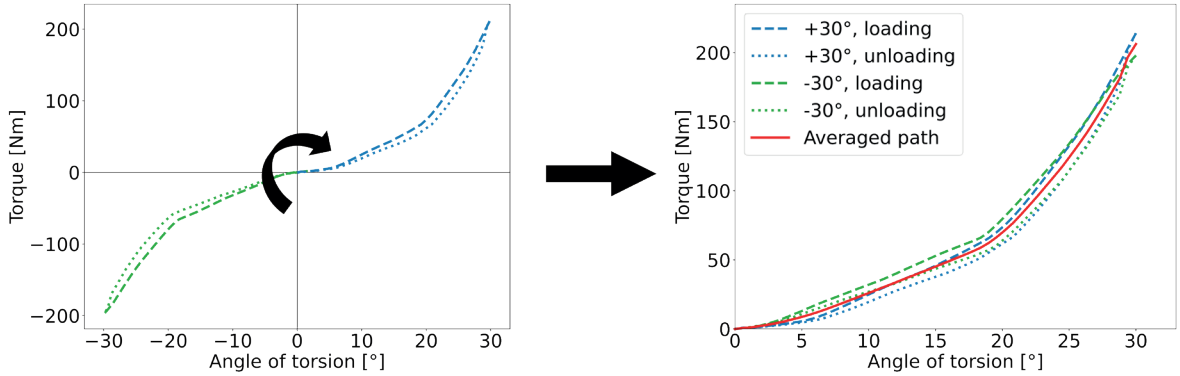


Fig. 4 Generation of average loading response characteristic from simulated results

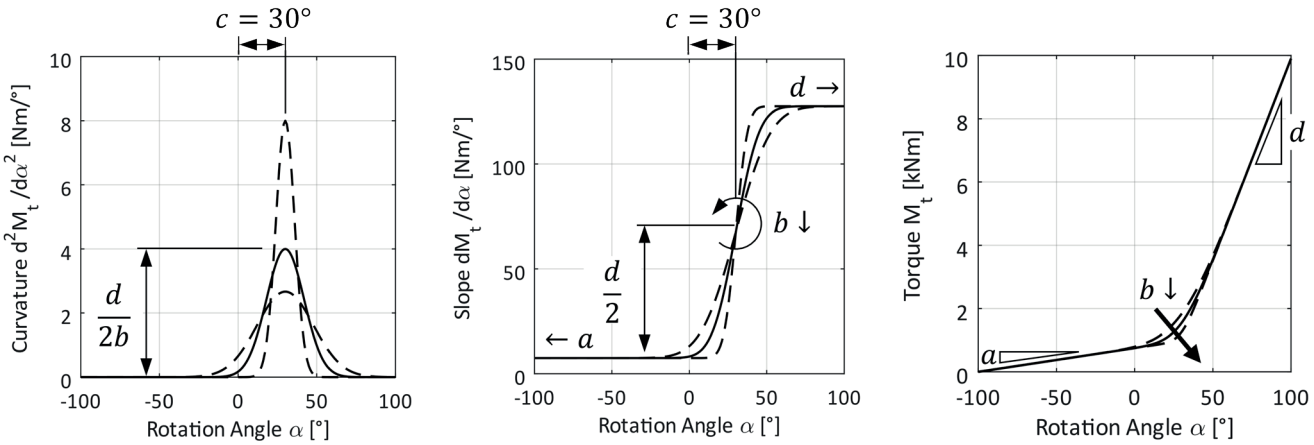


Fig. 5 Parametrization of model for $M_t(\alpha)$ according to Eq. (1). The dashed lines correspond to 50% higher (lower curvature), and 50% lower (higher curvature) b values, respectively. The slope at $\alpha = 30°$ is $a + d/2$

Following this approach, the surrogate model then does not directly fit the torque M_t vs. rotation angle α curve but rather the three modelling parameters a, b, c, and d. Thus, the fitting with the model Eq. (1) corresponds to a data-reduction step to reduce data complexity.

The actual surrogate model corresponds to three separate multi-linear regression models (RSM – Response Surface Models) fitting the model parameters a, b, and d (i.e. response variables y_k with $k = 1, 2, 3$) of Eq. (1), respectively their transformed values $f(y_k)$, in dependence of the six geometric parameters B_{IT}, B_{AT}, R_{AT}, D_{GK}, L^S_{GK}, and L^e_{GK} (i.e. predictors x_i with $i = 1, \ldots, 6$). In its most general form, an RSM includes a bias term $\beta_0^{(k)}$, linear terms $\beta_i^{(k)} x_i$, quadratic terms $\beta_{ii}^{(k)} x_i^2$, and interaction terms $\beta_{ij}^{(k)} x_i x_j$ with 28 model coefficients $\beta^{(k)}$ per response variable y_k as follows:

$$f(y_k) = \beta_0^{(k)} + \sum_{i=1}^{6} \beta_i^{(k)} x_i + \sum_{i=1}^{6} \sum_{j=1}^{6} \beta_{ij}^{(k)} x_i x_j + \sum_{i=1}^{6} \beta_{ii}^{(k)} x_i^2 \tag{2}$$

To stabilize variances ensuring the homoscedasticity assumption for linear regression, to reduce skewness of the data, and improve linearity, a log-transform $f(y_k) = \log(y_k)$ was applied for all response variables $y_k = a$, b, and d as indicated by the Q-Q plots in Fig. 6 comparing observed residuals with theoretical normal quantiles. The Q-Q plots for all response variables indicate an S-shape pointing to heavy tails and thus non-normality of the data. This is more pronounced for a and d and significantly improved by the log-transform. While for the response variable b the log-transform does not appear to be effective, the transformation is kept for consistency between the models. While the model resulting from the ordinary least squares (OLS) algorithm is still unbiased and trustworthy, the computed confidence and prediction intervals for b need to be treated with care.

To reduce the large number of three times 28 model parameters $\beta^{(k)}$ in Eq. (2), the least complex common model structure valid for all response variables y_k was identified, ensuring high variance clarification and low bias via high adjusted R^2 values. Best results were achieved using the following linear regression approach:

$$\log(y_k) = \beta_0^{(k)} + \beta_1^{(k)} \log\left(L^s_{GK}\right) + \beta_2^{(k)} R_{AT} + \beta_3^{(k)} B_{IT} + \beta_4^{(k)} B_{IT}^2 + \beta_5^{(k)} \log(D_{GK}) \tag{3}$$

Due to the high correlation between B_{AT} and B_{IT} as well as L^e_{GK} and L^S_{GK}, see Fig. 7, the former predictors have been dropped from the model Eq. (3) to meet the Gauss-Markov requirements of the OLS method. For the response variables $y_k = a$ and d the highest correlations are found for the remaining predictors L^S_{GK}, B_{IT}, and D_{GK}, i.e. the as-cut length of the rubber cord, the width of the inner square profile, and the diameter of the rubber cord, respectively. For the response variables $y_k = b$ the highest correlation was with the predictors D_{GK}, R_{AT}, and B_{AT}

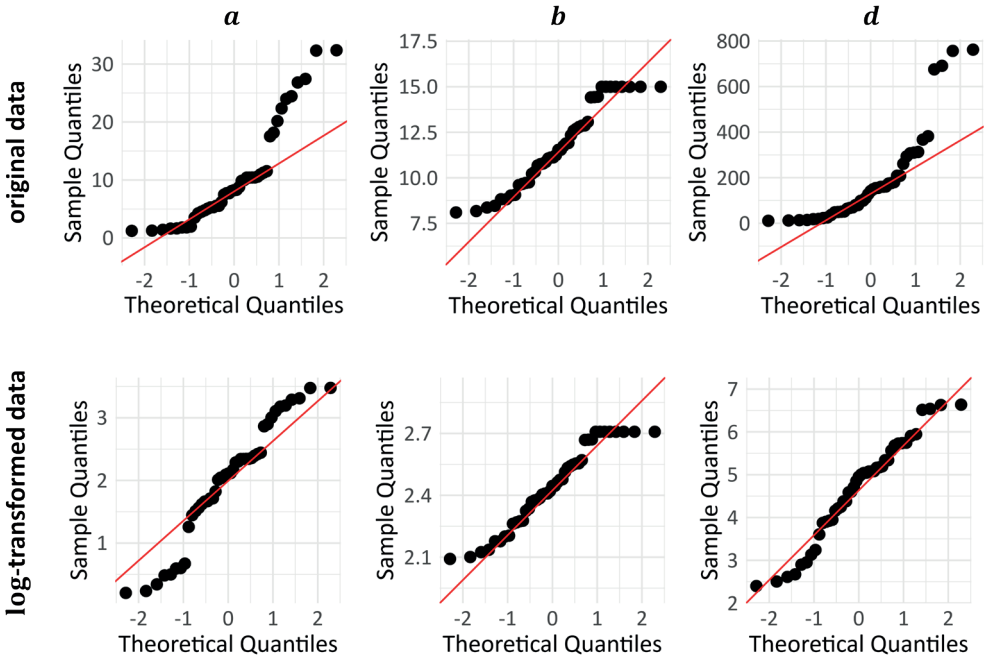


Fig. 6 Q-Q plots of original and as-log-transformed data for the model responses $y_k = a$, b, and d

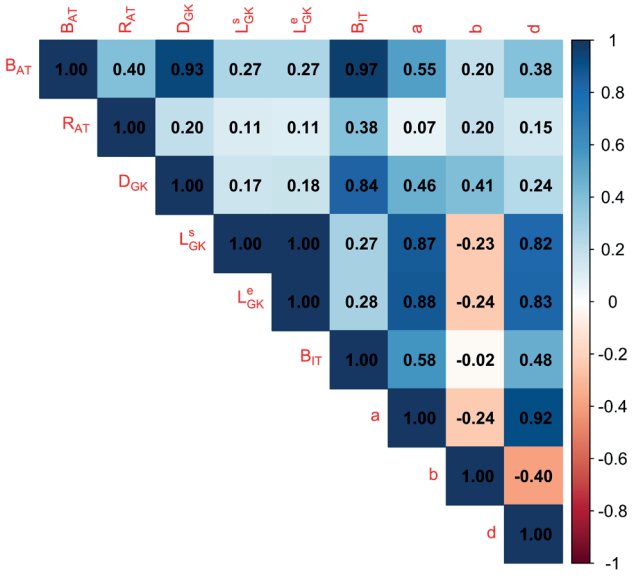


Fig. 7 Correlation matrix between predictors x_i (B_{IT}, B_{AT}, R_{AT}, D_{GK}, L^S_{GK}, and L^e_{GK}) and response variables y_k (a, b and d)

which was represented via B_{IT} given the strong correlation between these predictors. Furthermore, the response variables a and d show strong positive correlations while b is weakly negatively correlated to a and d. To verify the unbiasedness of the models, the Tukey-Anscombe plots were checked for zero mean and constant variance of the residuals, proving that the Gauss-Markov assumptions of the OLS method are met at an acceptable level.

The surrogate model is fitted on the training dataset using the open-source software *R*. Subsequently, the predictive performance of the regression model is tested based on the independent test dataset. Finally, the surrogate model uses the three-geometry parameter dependent regression models of the model parameters $y_k = a$, b and d as well as the model in Eq. (1) to predict geometry dependent loading responses (torque vs. rotation angle).

3 Results

3.1 Predictive performance of high-fidelity simulation model

A comparison of the high-fidelity model with experimental data for a ROSTA DR50x120 RSDE shows excellent agreement for the torsional loading characteristic, see Fig. 8. Simulated peak torques at $\alpha = \pm 30°$ are within ±3% of the measured values, while the predicted hysteresis area is significantly smaller than the experimentally determined values. Deviations of the loading characteristic lie well within the error band of ±15% (at $\alpha = \pm 30°$) indicating the variability caused by geometrical tolerances of the RSDE. While the model successfully predicts the average

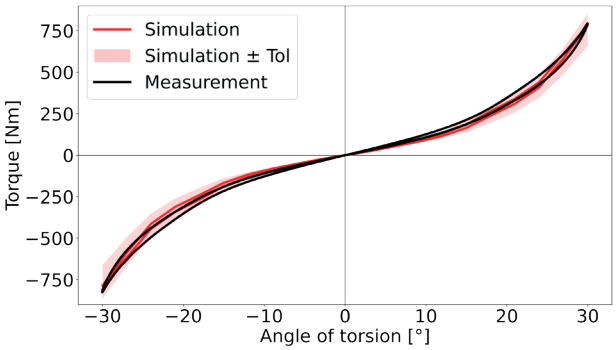


Fig. 8 Comparison of high-fidelity simulation with experimental loading characteristic of a ROSTA DR50x120 RSDE. The red error band describes the variability of the loading characteristic resulting from the specified geometry tolerances

loading characteristic, the dissipated energy (damping of RSDE) is insufficiently covered. This discrepancy is expected to be due to additional energy dissipation in the contact interface which may not be fully covered by the employed contact modelling approach. At this point it must be mentioned that the METM plus AMDM constitutive framework neglects rate-dependent material behavior. With AMDM hysteresis originates from the asymmetry between loading and unloading damage functions only. The hyperelastic material modelling itself is rate independent. However, this simplification was chosen on purpose, since carbon black filled vulcanizates generally show rather weak rate dependency for low and medium loading frequencies. In fact, under quasi-static loading conditions and after cyclic preconditioning, the stabilized equilibrium response is only weakly affected by strain rate compared with phenomena such as stress softening and filler-network rearrangement [17, 21, 22, 23].

While the model still allows for a qualitative comparison of the damping capacity of different geometry variants, the major focus for surrogate modelling is on determining the average cyclic stiffness of the torque vs. rotation angle characteristic where reasonable predictions are achieved.

3.2 Surrogate model

The various RSDE geometry variants of the training dataset have been fitted by the $M_t(\alpha)$ model in Eq. (1) with a goodness-of-fit level of $R^2 > 0.999$. Thus, the $M_t(\alpha)$ model provides excellent representation of the simulated loading response characteristics based on only three physically interpretable model parameters a, b, and d.

Similarly, the subsequent training of the response surface multi-linear regression model Eq. (3) for these three model parameters a, b and d yielded very good coverage

Table 3 Adjusted R^2 values of multi-linear response surface regression model Eq. (3) for response variables $y_k = a$, b and $b(k = 1, 2, 3)$ as input for the $M_t(\alpha)$ model in Eq. (1)

k	y_k	R^2_{adj}
1	a	0.977
2	b	0.832
3	d	0.966

of the data. Table 3 shows the respective adjusted R^2 values for the three different multi-linear response surface regression models Eq. (3). Due to confidentiality, the fitted model parameters are not published. The RSM models for a and d achieve a very high goodness-of-fit level with $R^2_{adj} > 0.96$, while it is a little lower for model for b at $R^2_{adj} > 0.83$. The reduced model coverage is likely to be due to the higher uncertainty associated with the fitting of b to the simulated loading characteristics. As the parameter c is fixed at 30° to reduce model complexity, this indicates that the maximum curvature (peak of $d^2M_t/d\alpha^2$ in Fig. 5) is defined to be at $|\alpha| = 30°$. While the slope at $|\alpha| = 30°$ is determined by $a + d/2$, the maximum curvature is given by $d/2b$. In cases where geometrical effects cause a significant shift of the curvature peak towards higher or lower angular displacements, there will be significant bias in the fitted b parameter masking the real effect of the geometry on the curvature. This is also indicated by the indifference of the -transform on the Q-Q plot of b in Fig. 6. The different goodness-of-fit levels for the model parameters a, b, and d is also reflected in the comparison of the RSM predictions with actual values for the training dataset and the independent test dataset in Fig. 9. Especially for larger a and d values, the discrepancy of the model predictions is larger, indicating worse predictions for stiffer RSDE as these values are representative of the stiffnesses at $|\alpha| = 0°$ and 30°. The parameter b controlling the curvature in the transition region is less well predicted by the RSM. Its effect on the loading response characteristics is, however, less important, i.e. about ±20% in the peak torque at $|\alpha| = 30°$, as shown by the dashed curves in Fig. 5 that represent a variation of b by ±50%.

Fig. 10 shows the partial residual plots for the for log-transformed response variables a, b, and d illustrating the effect of the different geometrical predictor variables L^S_{GK}, B_{IT}, D_{GK}, and R_{AT} defining the multi-linear response surface model Eq. (3). Due to the direct interpretability of the model parameters for the $M_t(\alpha)$ model in Eq. (1), the effect of the different geometric parameters on the loading response can be investigated. The as-cut length

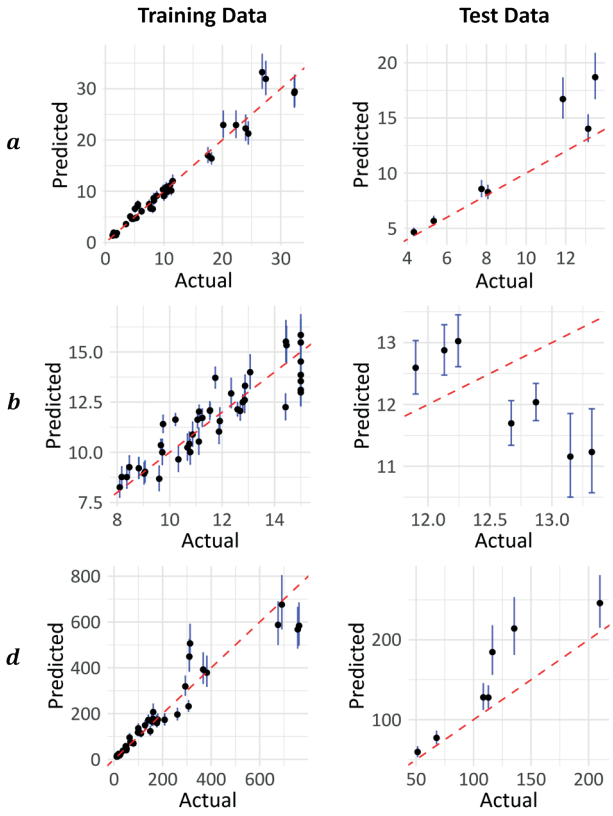


Fig. 9 Comparison of values for the $M_t(\alpha)$ model in Eq. (1) as predicted by the fitted multi-linear response surface model in Eq. (3) with actual values. Left column: training data. Right column: independent test data. Blue error bars describe 95% confidence intervals

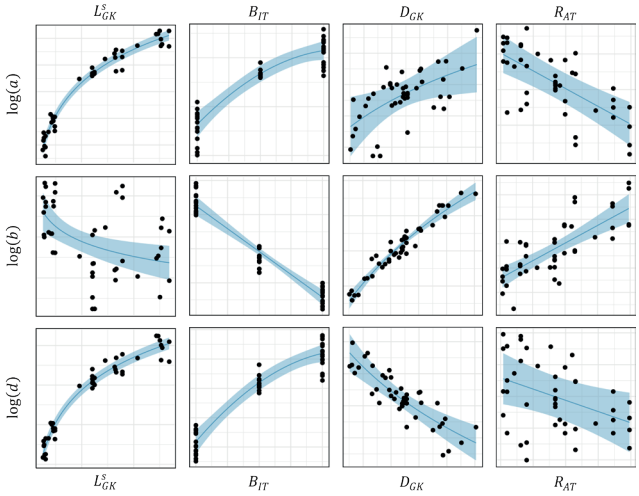


Fig. 10 Partial residual plots for -transformed response variables (y_k) as a function of the predictors x_i according to the multi-linear response surface regression model Eq. (3) showing the effect of the different predictors together with the 95% confidence interval (blue error band)

of the rubber cord L^S_{GK}, for instance, increases both the slope at $|\alpha| = 0°$ and 30°, while being more effective in increasing the stiffness at lower cord lengths. At the same time, it reduces the model parameter b which increases

the curvature in the transition regime. The width of the inner square profile B_{IT} has a similar, while less non-linear effect. An increase of the rubber cord diameter D_{GK}, on the other hand, increases the slope at $|\alpha| = 0°$, while reducing the slope at $|\alpha| = 30°$. The curvature, being proportional to $1/b$ decreases with larger cord diameters. An increasing corner radius of the outer profile R_{AT} further reduces both the slopes at $|\alpha| = 0°$ and 30° and the curvature in the transition regime. An increasing scatter from L^S_{GK} to B_{IT}, D_{GK}, and R_{AT} reflects the increasing variance and thus lower correlation coefficients listed in the correlation matrix in Fig. 7.

The parameters L^S_{GK} and D_{GK} define the geometry of the rubber cord yielding an increased volume of rubber for larger values that is pressed into the intermediate space between the inner and outer square profiles. Longer rubber cords, and thus longer RSDE, lead to an increased stiffness analogous to a larger number of springs connected in series. In general, an increased rubber volume at a fixed intermediate space between inner and outer profile, is expected to increase the stiffness both at $|\alpha| = 0°$ and 30°. The apparently lower slope at $|\alpha| = 30°$ for larger D_{GK} could, however, be explained by a smoother transition zone (which is supported by increased b values, i.e. lower curvatures) that implies that the maximum slope is not yet reached at $|\alpha| = 30°$ indicating a bias caused by fixing the model parameter c to 30° in Eq. (1). It could therefore be concluded, that an increased D_{GK} would extend the operational regime to beyond ± 30° until the maximum slope is reached.

The intermediate space between inner and outer profile, on the other hand, is defined by the width B_{AT} (which is at a fixed ratio to B_{IT} by design) and the radius R_{AT} of the outer square profile. A smaller R_{AT} thereby imposes a more rectangular shape of the pressed-in rubber cord at the contact to the outer profile, while a larger R_{AT} leads to a smoother elliptical shape. The associated stress state in the rubber cord appears to bring about larger stiffnesses at $|\alpha| = 0°$ and 30° for more heavily deformed rubber cords approaching a rectangular shape than for less extreme deformations during assembly.

Finally, the parameters of the $M_t(\alpha)$ model in Eq. (1) as represented by the multi-linear response surface model in Eq. (3) are used to predict the loading response of a ROSTA DR50x120 RSDE in the sense of a surrogate model. Fig. 11 compares the surrogate model prediction with the as-simulated loading characteristic showing good agreement within the tolerance-induced scatter band. This underpins the acceptable reliability and predictive performance of the surrogate model needed to make fast and robust estimates of the cyclic loading characteristics of non-linear RSDE.

4 Conclusions

This work presented a surrogate modelling framework for rubber spring and damping elements (RSDE) that combines high-fidelity finite element simulations with surrogate modelling to enable rapid prediction of cyclic stiffness characteristics. The developed methodology integrates a physically motivated constitutive description based on the Modified Extended Tube Model (METM) and Advanced Mullins Damage Modeling (AMDM) within a three-dimensional Abaqus UMAT implementation. By explicitly accounting for assembly-induced preload, stress softening, and equilibrium behavior after multiple loading cycles, the FE model provides a realistic representation of the steady-state mechanical response of filled vulcanizates. Validation against experimental measurements of a commercial RSDE demonstrated excellent agreement for the torque-angle characteristic, with deviations of peak torque remaining below ±3%.

To overcome the computational cost associated with high-fidelity simulations, a surrogate model was derived from a parameterized design-of-experiments study covering representative RSDE geometries. The simulated loading characteristics were condensed into three physically interpretable parameters that describe the evolution of cyclic stiffness over the operating range. These parameters were subsequently approximated by multi-linear response surface models linking the mechanical response to six geometric design variables. The resulting regression models achieved high predictive quality, with adjusted

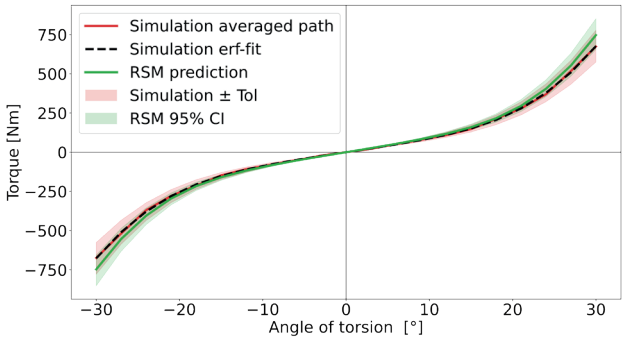


Fig. 11 Comparison of loading characteristics as predicted by the surrogate model with experimental loading characteristics of a ROSTA DR50x120 RSDE. The red error band describes the variability of the loading characteristic resulting from the specified geometry tolerances. The green error band describes the statistical 95% confidence interval

coefficients of determination of up to 0.977, demonstrating that the dominant effects of geometry on cyclic stiffness can be represented reliably by a comparatively simple analytical model.

The analysis revealed that the geometry of the rubber cords and profile dimensions strongly influence the stiffness progression under torsional deformation. In particular, rubber cord length, diameter, and the dimensions of the steel profiles govern both the initial stiffness and the transition towards higher stiffness levels at larger angular deflections. These findings provide valuable engineering insight into the design mechanisms of RSDE and support the development of application-specific solutions without extensive prototyping or physical testing.

The proposed surrogate model therefore provides real-time predictions of geometry-dependent cyclic loading characteristics within the investigated design space. Such a tool can significantly accelerate the design and optimization of rubber-based vibration isolation systems and provides a practical basis for the future development of digital twins for complete rubber spring and damping systems (RSDS) including e.g. sensors for condition monitoring of vibrating systems. In addition, the proposed surrogate model enables early-stage design exploration and optimization of RSDE without extensive prototyping, thereby reducing development time and testing effort in industrial vibration-isolation applications.

Future work should focus on extending the approach beyond stiffness characterization by improving the prediction of damping behavior and hysteresis losses. This will likely require enhanced contact modelling as well as the incorporation of rate-dependent viscoelastic effects. Furthermore, extending the surrogate model to different rubber compounds and a wider geometric parameter space would improve its applicability and robustness for industrial design tasks. Ultimately, coupling the RSDE surrogate model with system-level models of complete RSDS offers promising opportunities for virtual prototyping, optimization, and predictive engineering of vibration isolation systems.

Acknowledgements

The authors acknowledge the financial support of Innosuisse – Swiss Innovation Agency for the project 102.422 IP-ENG as well as the project partners ROSTA AG and Compounds AG for supporting this research.

References

[1] Falkner, P., Fimbinger, E., Flachberger, H. "Virtual Prototyping of the RM Active Grid®: a DEM-MBD Study", BHM Berg- Hüttenmänn. Monatshefte, 169(8), pp. 400–411, 2024. https://doi.org/10.1007/s00501-024-01493-1

[2] Cieplok, G. "Influence of vibratory conveyor design parameters on the trough motion and the self-synchronization of inertial vibrators", Open Engineering, 14(1), 20220434, 2024. https://doi.org/10.1515/eng-2022-0434

[3] Kamioka, T., Shin, H., Yamaguchi, R., Muromachi, M. "Development and Analysis of a Biped Robot with Prismatic Compliance", In: 2022 International Conference on Robotics and Automation (ICRA), Philadelphia, PA, USA, 2022, pp. 10398–10404. ISBN 978-1-7281-9681-7 https://doi.org/10.1109/ICRA46639.2022.9811962

[4] Kritzinger, W., Karner, M., Traar, G., Henjes, J., Sihn, W. "Digital Twin in manufacturing: A categorical literature review and classification", IFAC-PapersOnline, 51(11) , pp. 1016–1022, 2018. https://doi.org/10.1016/j.ifacol.2018.08.474

[5] Cârdei, P., Munteanu, AI., Muraru, V., Sfiru, R. "Elementary Nonlinear with Linear Damping Mathematical Model for Neidhart Suspension", INMATEH - Agricultural Engineering, 30(1), pp. 31–34, 2010. [Online] Available at: https://www.inma-ita.ro/inmateh/INMATEH%20I_2010/INMATEH%20I%20-%202010_rev.pdf [Accessed: 20. October 2026]

[6] Cieplok, G., Wójcik, K., Michalczyk, K., Sikora, W. "Equivalent Parameters of Metal-Elastomer Vibroinsulators", Vibrations in Physical Systems, 31(2), pp. 2020204-1–2020204-13, 2020. http://doi.org/10.21008/j.0860-6897.2020.2.04

[7] Koini, D., Fimbinger, E. "Modelling the Dynamics of Oscillating Mountings with a Pantograph Structure Using Simulink: A Case Study on Rosta Ab Spring-Damper Elements", Results in Engineering, 26, 105529, 2025, https://doi.org/10.1016/j.rineng.2025.105529

[8] Sikora, W., Michalczyk, K., Machniewicz, T. "Numerical Modelling of Metal-Elastomer Spring Nonlinear Response for Low-Rate Deformations", Acta Mechanica et Automatica, 12(1), pp. 31–37, 2018. https://doi.org/10.2478/ama-2018-0005

[9] Wu, J., Liu, C., Jiang, H., Wang, Z. "Numerical modeling and experimental testing analysis of Assembled Rubber Metal Isolator", Science Progress, 103(3), 2020. https://doi.org/10.1177/0036850420956985

[10] Sikora, W., Michalczyk, K., Machniewicz, T. "A Study of the Preload Force in Metal-Elastomer Torsion Springs", Acta Mechanica et Automatica, 10(4), pp. 300–305, 2016. https://doi.org/10.1515/ama-2016-0047

[11] Zhang, Y., Zhang, H., Liu, Z., Zhu, P. "A novel surrogate modeling strategy for the mechanical performance of CFRP/Al multi-riveted-bonded joints based on an innovative sampling scheme", Composite Structures, 363, 119140, 2025. https://doi.org/10.1016/j.compstruct.2025.119140

[12] Kumar, A., Sridhara, S., Suresh, K. "A novel surrogate model for optimizing lattice for desired force-displacement response", Engineering with Computers, 42, 169, 2026. https://doi.org/10.1007/s00366-026-02407-0

[13] Montgomery, D. C., Peck, E. A., Vining, G. G. "Introduction to Linear Regression Analysis", John Wiley & Sons, 2021, ISBN 978-1-119-57872-7

[14] Myers, R. H., Montgomery, D. C., Anderson-Cook, C. M. "Response Surface Methodology: Process and Product Optimization Using Designed Experiments", John Wiley & Sons, 2016, ISBN 978-1-118-91601-8.

[15] Impollonia, N., Sofi, A. "A response surface approach for the static analysis of stochastic structures with geometrical nonlinearities", Computer Methods in Applied Mechanics and Engineering, 192(37–38), pp. 4109–4129, 2003. https://doi.org/10.1016/S0045-7825(03)00379-7

[16] Wrana, C., Eberlein, R. "Modification of the Extended Tube Model (METM) for the Characterization of Filled Vulcanizates", Rubber Chemistry and Technoligy, 97(3), pp. 205–224, 2024. https://doi.org/10.5254/rct.24.00021

[17] Wrana, C., Eberlein, R. "Advanced Mullins Damage Modeling (AMDM) after Multiple Cyclic Loading in Vulcanizates; Part 1: Theory and Parameter Identification", Rubber Chemistry and Technoligy, 98(1), pp. 124–141, 2025. https://doi.org/10.5254/rct.24.00047

[18] Eberlein, R., Wrana, C. "Non-Linear Finite Element Damage Modeling after Multiple Cyclic Loading of Rubberlike Materials", International Journal of Non-Linear Mechanics, 178, 105170, 2025. https://doi.org/10.1016/j.ijnonlinmec.2025.105170

[19] Ogden, R. W., Roxburgh, D. G. "A pseudo–elastic model for the Mullins effect in filled rubber", Proceedings of the Royal SocietyA, 455(988), pp. 2861–2877, 1999. https://doi.org/10.1098/rspa.1999.0431

[20] Box, G. E. P., Wilson, K. B. "On the Experimental Attainment of Optimum Conditions", Journal of the Royal Statistical Society: Series B (Methodological), 13(1), pp. 1–38, 1951. https://doi.org/10.1111/j.2517-6161.1951.tb00067.x

[21] Bergström, J.S., Boyce, M.C. "Constitutive modeling of the large strain time-dependent behavior of elastomers", Journal of the Mechanics and Physics of Solids, 46(5), pp. 931–954, 1998. https://doi.org/10.1016/S0022-5096(97)00075-6

[22] Lion, A. " On the large deformation behaviour of reinforced rubber at different temperatures", Journal of the Mechanics and Physics of Solids, 45(11–12), pp. 1805–1834, 1997. https://doi.org/10.1016/S0022-5096(97)00028-8

[23] Diani, J., Fayolle, B., Gilormini, P. "A review on the Mullins effect", European Polymer Journal, 45(3), pp. 601–612, 2009. https://doi.org/10.1016/j.eurpolymj.2008.11.017